XVI International Conference on Durability of Building Materials and Components
DBMC 2023, China
K.F. Li and D.P. Fang (Eds)

An In-situ Method for Assessing the Kinetics of Acid Attack on Iron-rich Alkali-activated Materials

Ziyou Yu[1], Rodrigo de Oliveira-Silva[1], Everton De Oliveira[1], Nana Wen[2], Yiannis Pontikes[2], Dimitrios Sakellariou[1]

[1]KU Leuven, M2S, cMACS, Celestijnenlaan 200F, Leuven 3001, Belgium, ziyou.yu@kuluven.be (Ziyou Yu), rodrigo.deoliveirasilva@kuleuven.be (Rodrigo de Oliveira-Silva), everton.deoliveira@kuleuven.be (Everton De Oliveira), dimitrios.sakellariou@kuleuven.be (Dimitrios Sakellariou)

[2]KU Leuven, Department of Materials Engineering, Kasteelpark Arenberg 44, Leuven 3001, Belgium, nana.wen@kuleuven.be (Nana Wen), yiannis.pontikes@kuleuven.be (Yiannis Pontikes)

Abstract. *In iron-rich alkali-activated materials (AAMs), iron is present in both the ferrous and ferric states. Fe^{3+} is considered to be present in a silicate network and the dissolution of Fe^{3+} under acid attack can be taken as an indication of the deterioration of the AAMs framework. Conventional methods for evaluating the acid resistance of AAMs are based on the durability standards for OPC concrete with indicators such as mass change and dimensional change, or by measuring the corroded depth. All of these methods are measured based on solid samples and many samples have to be prepared to obtain different points in a time profile. Here we propose nuclear magnetic resonance (NMR) relaxometry measurements as an in-situ method for the direct determination of dissolution kinetics of Fe^{3+} ions in an acid solution with high temporal resolution. The leaching kinetics of iron-rich AAMs in (sulfuric) acid can be described by the Real Physical Picture (RPP) kinetic model, which was originally used to describe the gas-solid interaction. The fitting results show that the leaching process is controlled by chemical reactions at the beginning and by diffusion over time.*

Keywords: *Iron-rich AAMs, Low-field NMR, Acid Attack, In-situ Kinetics, RPP Model.*

1 Introduction

Iron-rich alkali-activated materials (AAMs) have emerged as an interesting alternative to ordinary Portland cements (OPCs) due to their potential to offer improved performance and environmental benefits. Previous research has shown that alkali-activated non-ferrous slag usually exhibits high compressive strength and is thus the most promising solution for slag valorization in iron-rich AAMs (Ponomar et al. 2022). In order to apply iron-rich AAMs on a large scale and commercially, their long-term durability must be evaluated. In several applications and environments, concrete and cementitious materials are exposed to acidic solutions. For example, sulfuric acid attack is the main cause of structural material degradation in sewer pipes carrying waste water, acid mine drainage areas, biogas plants, and power plant cooling towers (Gluth et al. 2022). In this paper, the resistance of iron-rich AAMs to the sulfuric acid attack was investigated.

Conventional methods for evaluating the acid resistance of AAMs are based on the durability standards for OPC concrete, such as mass change, visual inspection, change in cross-sectional dimensions, and compressive strength. However, these standards are not universal for all the AAMs, as demonstrated by (Aliques-Granero et al. 2016). Corroded depth is considered as a

more accurate indicator of the progress of acid attack(Lloyd et al. 2012). However, due to the damage caused by removing the corroded layer, many samples must be prepared to obtain different points in a time profile, making the measurement error relatively high. In addition to making measurements on solid samples, it is also possible to monitor the concentration of specific atoms in acid solutions over time. Inductively Coupled Plasma Optical Emission spectrometry (ICP-OES) has been proposed to analyze the concentration of dissolved species (i.e., Si, Al, Ca, Fe, K/Na) in sulfuric acid to investigate the dissolution kinetics of AAMs (Grengg et al. 2021). In iron-rich AAMs, iron is present in both the ferrous (Fe^{2+}) and ferric (Fe^{3+}) states, adding to the complexity of the structure. Previous studies (Peys et al. 2019, Ponomar et al. 2022) have suggested that Fe^{3+} is present in a silicate network while Fe^{2+} is present in the form of trioctahedral $Fe(OH)_2$-like layers. Under acid attack, the dissolution of Fe^{3+} can be taken as an indication of the deterioration of the AAMs framework. However, ICP can only measure the total iron concentration (the sum of Fe^{2+} and Fe^{3+} concentrations). In order to obtain the concentration of Fe^{3+} ions, indirect method such as chelatometric titration (Bézos and Humler 2005) has to be carried out.

Here, we propose an *in situ* method to evaluate the leaching kinetics of iron-rich AAMs by directly measuring the change in Fe^{3+} ion concentration in an acid solution over time. The experiments were carried out using nuclear magnetic resonance (NMR) relaxometry by continuously measuring the transverse relaxation time T_2 over time. Previous research (Mitreiter et al. 2010) showed that the ^1H relaxation rate ($1/T_2$) in acid solutions is linearly correlated to the concentration of Fe^{3+} ions. This method enables capturing the changes in the Fe^{3+} ion concentration with high temporal resolution, providing more accurate degradation kinetics of AAMs. We have applied the Real Physical Picture (RPP) model (Chou and Hou 2009) (Wang et al. 2021), which was originally developed to describe gas-solid interactions, to our results. It is capable of accurately depicting the kinetic process of acid attack on iron-rich AAMs.

2 Background and Theory

2.1 Relaxation in Solution with Paramagnetic Ions

In solutions, the relaxation times of ^1H are affected by viscosity, molecular motion (temperature), and especially the amount of paramagnetic species, such as the dissolved Fe^{3+} ions. The theoretical background to these effects on relaxation in liquids is described by the Bloembergen-Purcell-Pound (BPP) theory (Bloembergen et al. 1948). In the presence of Fe^{3+} ions in liquid, the relaxation rate consists of two contributions: the diamagnetic and the paramagnetic contribution, as expressed by Equation (1):

$$\frac{1}{T_{2b}} = \frac{1}{T_{2d}} + R_{2p} \cdot c_p \tag{1}$$

where T_{2b} is the observed transverse relaxation time, T_{2d} is the transverse relaxation time of diamagnetic component (such as water), c_p is the concentration of paramagnetic ions, and R_{2p} is the relaxivity of paramagnetic ions.

The diamagnetic component $\frac{1}{T_{2d}}$ is a constant, the observed relaxation rate $\frac{1}{T_{2b}}$ is linearly

proportional to the concentration of paramagnetic ions in solution. This is the basic theory for correlating the relaxation times of solution with the concentration of paramagnetic ions in the solution.

2.2 NMR Pulse Sequences

The transverse relaxation time of water can be determined by a series of radio-frequency (RF) pulses, i.e., the Carr-Purcell-Meiboom-Gill (CPMG) echo train (Meiboom and Gill 1958). After an initial excitation of the magnetization by a $\pi/2$ RF pulse a spin echo train is generated by π RF pulses (Figure 1). The sequence parameters were set as: number of echoes = 32, echo time (2τ) = 300 μs, $\pi/2$ pulse length = 10 μs, and relaxation recycle delay = 2 s.

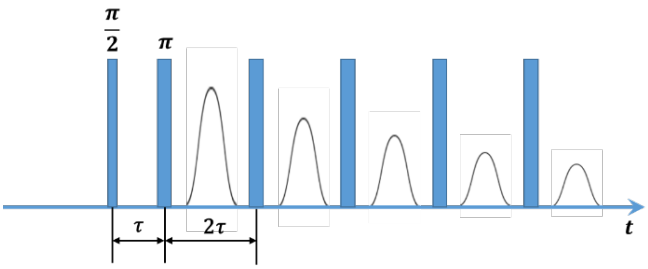

Figure 1. Pulse sequence CPMG for measuring T_2.

2.3 Real Physical Picture (RPP) Model

The Real Physical Picture (RPP) model was adopted in our work to describe the dissolution kinetics of Fe^{3+} in sulfuric acid water solution. This model was developed by (Chou and Hou 2009) to describe the gas-solid interface reactions with an emphasis on different rate-controlling steps, i.e., diffusion and chemical reaction. This model considers the geometry dimensions of materials. For a sample with cylindrical shape, the kinetic formula can be expressed as follows.

a. Dissolution controlled by diffusion:

$$\xi = 1 - \left[1 - \frac{h_0}{2R_0}\sqrt{\frac{t}{t_d}}\right]^2 \left[1 - \sqrt{\frac{t}{t_d}}\right] \tag{2}$$

b. Dissolution controlled by chemical reaction:

$$\xi = 1 - \left[1 - \frac{h_0}{2R_0}\frac{t}{t_c}\right]^2 \left[1 - \frac{t}{t_c}\right] \tag{3}$$

where ξ the reacted fraction, t is reaction time, h_0 is the height of the cylinder, $2R_0$ is the diameter of the cylinder, t_c and t_d are the 'characteristic reaction times', which can be expressed as parameters with clear physical meaning by (Chou and Hou 2009). When $t = t_c$ or t_d , one has $\xi = 1$. Therefore, t_c and t_d are the time required for the whole cylinder to undergo complete reaction and can be suggested to evaluate the acid resistance of AAMs.

3 Materials and Methods

The precursor used in this work was synthesized slag with the chemical composition given in Table 1. The procedure for the synthesis of the slag is referred to in (Wen et al. 2021). The alkali activating solution ($Na_2O{\cdot}1.65\ SiO_2$, with 65% H_2O) was prepared by dissolving sodium hydroxide pellets in a commercial sodium silicate ($Na_2O{\cdot}3.3\ SiO_2$ with 63.5 wt% H_2O) and deionized water. The AAM paste was prepared with an activator/slag ratio of 0.4. The paste was cured in a sealed 1.3 mm diameter cylindrical mold for 28 days. After curing, the cylindrical sample was cut into small discs of 5 mm height for further acid attack testing. The redox of iron (Fe^{2+}/Fe^{3+}) in the synthesized AAM is 6.20, which was measured by NMR relaxometry.

Table 1. Chemical composition of the synthetic slag (mol%).

	FeO	SiO_2	Al_2O_3	CaO
Slag	41	35	5	19

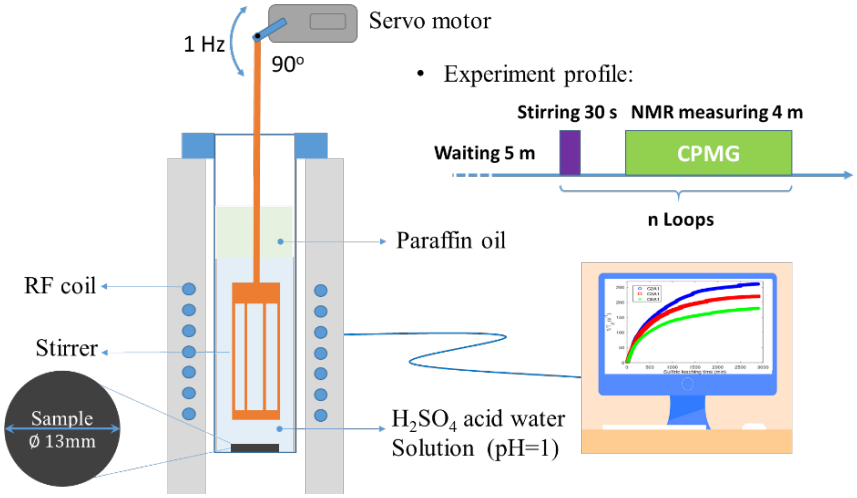

Figure 2. Experiment set-up and measurement profile

The acid attack experiments were carried out on a home-made 0.2 T NMR relaxometer where the magnetic field was produced by a homogeneous Halbach-like magnet. Magnet and sample were temperature-stabilized at 28 °C. As shown in Figure 2, the AAM disc was placed at the bottom of the NMR glass tube containing 50 ml, pH=1 sulfuric acid water solution. The solid sample was placed outside the RF coil while only the relaxation times from the solution were measured. The timing of the experiment started when the solid and liquid came into contact. After 5 minutes of contact, the solution was stirred for 30 seconds to achieve homogeneity before the NMR measurement. The frequency of the up-and-down stirring is 1 Hz, controlled by a servo motor with a rotation angle of 90°. After stirring, the solution was allowed to stand for 30 seconds to prevent liquid flow. The CPMG measurement lasted 4 minutes and the average T_2 was measured over this period. At the end of the NMR experiment, stirring was resumed and the previous steps were repeated. It is capable of collecting up to 12 points in an hour and offers a high level of temporal resolution.

4 Results and Discussion

4.1 Fe^{2+} and Fe^{3+} Ions in Solution

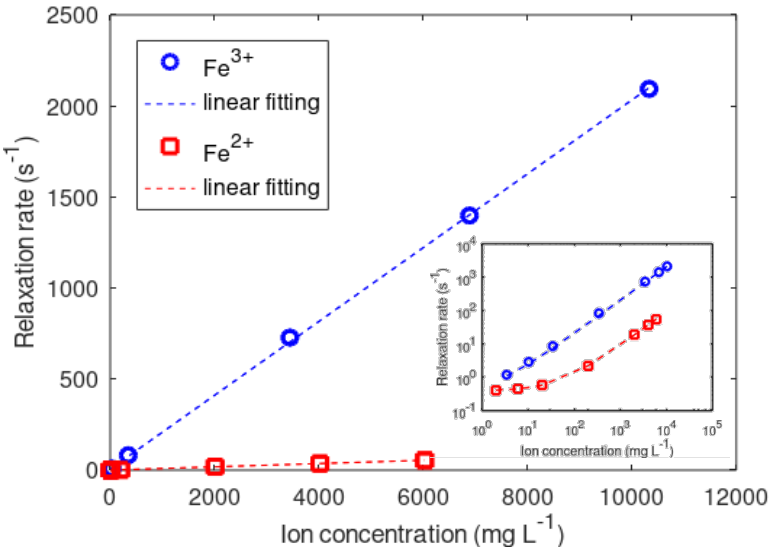

Figure 3. The dependence of the bulk water relaxation rate $1/T_2$ on the concentration of dissolved ions (Fe^{3+} and Fe^{2+}) in pH = 1 sulfuric acid solutions at 28 °C. The dashed lines are the linear fit calibration plot. The inset is the plot on a logarithmic scale.

The transverse relaxation rate ($1/T_2$) of sulfuric acid solutions containing Fe^{2+} and Fe^{3+} ions at pH = 1 was measured by CPMG sequence. The concentration of Fe^{2+} and Fe^{3+} ions ranges from 0 mg/L up to 10000 mg/L. Figure 3 shows the dependence of $1/T_2$ on the concentration of Fe^{2+} and Fe^{3+} ions in solutions. $1/T_2$ is linearly proportional to the concentration of Fe^{2+} and Fe^{3+} ions, in agreement with the BPP theory. By doing the linear fitting, we could extract the relaxivities of Fe^{2+} and Fe^{3+} ions (i.e., R_{2p} in Equation (1)), which are 0.0090 $\frac{s^{-1}}{mg\ L^{-1}}$ and 0.2034 $\frac{s^{-1}}{mg\ L^{-1}}$, respectively. $\frac{1}{T_{2d}}$ in the equation is set as the relaxation rate of bulk water in solution without iron ions, which is 0.3895 s^{-1}. As can be noticed that the contribution of Fe^{2+} ions to the relaxation is limited compared to that of Fe^{3+} ions, which exhibits two orders of magnitude higher contribution. In a solution containing both Fe^{2+} and Fe^{3+} ions, the contribution of Fe^{2+} ions to the relaxation can be neglected. Therefore, the relaxation rate measured by relaxometry can be directly related to the concentration of Fe^{3+} ions in a solution according to the following relationship:

$$\frac{1}{T_{2b}}(s^{-1}) = 0.3895(s^{-1}) + 0.2034\left(\frac{s^{-1}}{mg\ L^{-1}}\right)\cdot c_{Fe^{3+}}(mg\ L^{-1}) \text{ with } R^2 = 0.9998 \quad (4)$$

4.2 Fe^{3+} Dissolution Behavior in Sulfuric Acid Solution

The evolution of the transverse relaxation rate ($1/T_2$) of the bulk water in the sulfuric acid solution during the first day (1440 minutes) of the attack was recorded with high temporal resolution. The temporal progression is shown in Figure 4 as open circles (○). The relaxation rate was converted to the concentration of Fe^{3+} ions (shown on the right axis) in the acid solution according to Equation (4). During the first couple of hours, a rapid increase in the concentration of Fe^{3+} ions is observed, later the increase in Fe^{3+}-ion concentration slows down. Finally, it will converge towards an asymptotic value. The dissolution behavior of Fe^{3+} ions from the AAM framework suggests sulfuric acid attack kinetics on iron-rich AAMs.

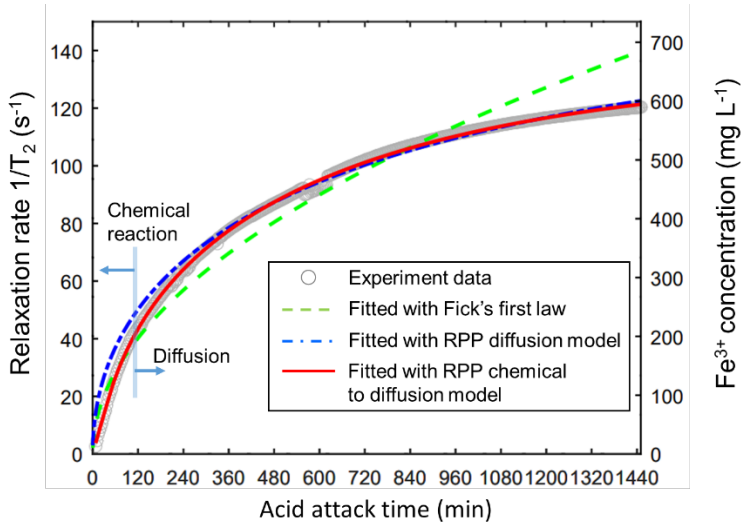

Figure 4. The kinetic process of sulfuric acid attack. Open circle (○) represents the experiment data and the solid lines are the simulation results based on Fick's first law (green dashed line) and RPP model (blue dash-dotted line fitted by Equation (2) and red solid line fitted by Equation (2,3)). Left: the transverse relaxation rate $1/T_2$ in s^{-1}. Right: the calculated Fe^{3+} ion concentration in mg L^{-1} in sulfuric acid solution based on Equation (4).

4.3 Kinetics Modeling of the Sulfuric Acid Attack on AAM Paste

Using the high temporal resolution provided by NMR relaxometry, we were able to fit kinetic models to the data. The green dashed line in Figure 4 was fitted by Fick's first law, which is a general model used to describe the diffusion behavior of a solute through a stationary medium. It can be seen that the fitting result is in relatively poor agreement with the experimental data. Taking into account the geometric dimensions of the sample (cylindrical shape), the experimental data were also fitted by the RPP diffusion model in Equation (2) (the blue dash-dotted line in Figure 4). Compared to Fick's first law, the RPP model is found to fit better. However, a deviation between the experimental data and the fitted line can be noticed at the onset of dissolution, indicating that the dissolution process is not controlled by ion diffusion at the beginning. The data was then fitted using Equation (2) and (3), taking into account both chemical reaction and diffusion rate control. The fit (red solid line in Figure 4) has a high degree of agreement with the experimental data with a residual standard error (R^2) of 0.9991. Therefore, the dissolution kinetics of Fe^{3+} ions is rate-controlled by chemical reaction at the onset and by diffusion over time. Parameters such as t_t (the transition time, 53 minutes), t_c (1.64×10^5

minutes), and t_d (1.18×10^5 minutes) can be derived from the fitting. These parameters are interpreted as follows: Before 53 minutes, the dissolution of Fe^{3+} ions is rate-controlled by the chemical reaction occurring on the interface, while after 53 minutes, ion diffusion (either H^+ ions diffusing into the solid or Fe^{3+} ions diffusing out towards the solution) controls the dissolution rate. The dissolution will take 1.64×10^5 minutes (~3.80 months) and 1.18×10^5 minutes (~ 2.73 months), respectively, to reach the end of the reaction if only chemical reaction or diffusion is considered as the rate-controlling step. The result obtained from the diffusion model is consistent with the results obtained from micro-CT, where we measured the corroded layer thickness for the same sample in this paper every month after immersion in the pH 1.0 H_2SO_4 solution (unpublished work). It shows that the corroded thickness reached 5 mm during the second to third month after acid attack.

The dissolution process can be schematically illustrated in Figure 5 based on the kinetic analysis. In a time profile, the dissolution process starts with the adsorption of H^+ on the surface of the solid, followed by the chemical reaction on the surface. The chemical reaction releases Fe^{3+} ions into the solution, inducing a shorter T_2. As the cations (not only Fe^{3+} but also Na^+, Ca^{2+}, Al^{3+}, etc.) are depleted, voids and cracks can form on the surface, facilitating the penetration and diffusion of H^+ ions into the solid. Chemical reactions will take place at the liquid-solid interface. The generated Fe^{3+} ions will diffuse out towards the solution. Compared to the chemical reaction, ion diffusion is slower and becomes the rate-controlling step in this process.

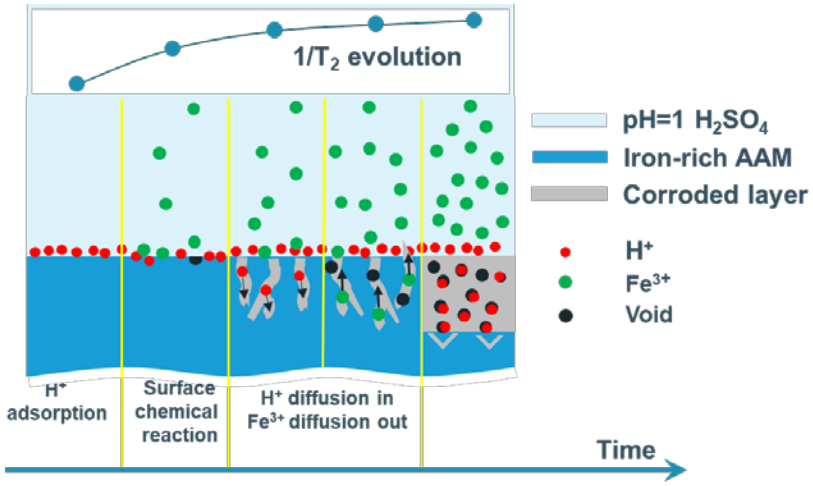

Figure 5. A schematic illustration of the dissolution of Fe^{3+} ions from the iron-rich AAM.

5 Conclusions

An in-situ method with a high temporal resolution for assessing the kinetics of acid attack on iron-rich AAMs has been proposed. By measuring the evolution of the transverse relaxation rate of the acid solution using NMR relaxometry, the dissolved concentration of Fe^{3+} ions can be calculated based on the BPP theory. The dissolution of Fe^{3+} ions indicates the deterioration of the framework of the AAM. The kinetics of degradation/dissolution can be described by the RPP model, which shows that the process is controlled by chemical reaction in the first few hours and by diffusion over time. The time required to complete the attack process is predicted

by the characteristic time t_d. In this work, the AAM was produced from a synthetic slag. Further experiments will be carried out on AAM produced from commercial slags containing iron oxides.

Acknowledgements

This project was supported by the KU Leuven Grant STG-18-00289 and by the Research Foundation Flanders (FWO) under Grant PorMedNMR − No. G0D5419N.

ORCID

Ziyou Yu: https://orcid.org/0000-0002-1662-9968
Rodrigo de Oliveira-Silva: https://orcid.org/0000-0003-3903-2678
Everton de Oliveira: https://orcid.org/0000-0003-1353-918X
Nana Wen: https://orcid.org/0000-0003-1657-7800
Yiannis Pontikes: https://orcid.org/0000-0002-2210-5394
Dimitrios Sakellariou: https://orcid.org/0000-0001-7424-5543

References

Ponomar, V., Yliniemi, J., Adesanya, E., Ohenoja, K. and Illikainen, M. (2022). *An overview of the utilisation of Fe-rich residues in alkali-activated binders: Mechanical properties and state of iron*. Journal of Cleaner Production 330, 129900.

Gluth, G., Grengg, C., Ukrainczyk, N., Mittermayr, F. and Dietzel, M. (2022). *Acid resistance of alkali-activated materials: recent advances and research needs*. RILEM Technical Letters 7, 58-67.

Aliques-Granero, J., Tognonvi, T. M. and Tagnit-Hamou, A. (2016). *Durability test methods and their application to AAMs: case of sulfuric-acid resistance*. Materials and Structures 50(1), 36.

Lloyd, R. R., Provis, J. L. and van Deventer, J. S. J. (2012). *Acid resistance of inorganic polymer binders. 1. Corrosion rate*. Materials and Structures 45(1), 1-14.

Grengg, C., Gluth, G. J. G., Mittermayr, F., Ukrainczyk, N., Bertmer, M., Guilherme Buzanich, A., Radtke, M., Leis, A. and Dietzel, M. (2021). *Deterioration mechanism of alkali-activated materials in sulfuric acid and the influence of Cu: A micro-to-nano structural, elemental and stable isotopic multi-proxy study*. Cement and Concrete Research 142, 106373.

Peys, A., Douvalis, A. P., Hallet, V., Rahier, H., Blanpain, B. and Pontikes, Y. (2019). *Inorganic Polymers From CaO-FeOx-SiO2 Slag: The Start of Oxidation of Fe and the Formation of a Mixed Valence Binder*. Frontiers in Materials 6.

Bézos, A. and Humler, E. (2005). *The Fe3+/ΣFe ratios of MORB glasses and their implications for mantle melting*. Geochimica et Cosmochimica Acta 69(3), 711-725.

Mitreiter, I., Oswald, S. E. and Stallmach, F. (2010). *Investigation of iron (III)-release in the pore water of natural sands by NMR relaxometry*. Open Magn Reson J 3(1), 46-51.

Chou, K. C. and Hou, X. M. (2009). *Kinetics of High‐Temperature Oxidation of Inorganic Nonmetallic Materials*. Journal of the American Ceramic Society 92(3), 585-594.

Wang, E., Hou, X., Chen, Y., Fang, Z., Chen, J., Liang, T., Chou, K.-c. and Nickel, K. G. (2021). *Progress in cognition of gas-solid interface reaction for non-oxide ceramics at high temperature*. Critical Reviews in Solid State and Materials Sciences 46(3), 218-250.

Bloembergen, N., Purcell, E. M. and Pound, R. V. (1948). *Relaxation Effects in Nuclear Magnetic Resonance Absorption*. Physical Review 73(7), 679-712.

Meiboom, S. and Gill, D. (1958). *Modified spin‐echo method for measuring nuclear relaxation times*. Review of scientific instruments 29(8), 688-691.

Wen, N., Peys, A., Hertel, T. and Pontikes, Y. (2021). *The effect of the chemical composition of MgO-CaO-FeO-Al2O3-SiO2 slag on the reaction kinetics and compressive strength of alkali-activated materials*. Proceedings of the 7th International Slag Valorisation Symposium, Leuven, Belgium.